

# Spectral Analysis of a Chaotic Map Based on the Hyperbolic Tangent Function

Carlos E. C. Souza, João V. C. Evangelista, Daniel P. B. Chaves e Cecilio Pimentel

**Abstract**—This work generalizes the chaotic map recently introduced by the authors with the addition of two new control parameters. The Lyapunov exponent is employed to analyze the chaotic dynamics of the proposed map. The spectral characteristics of chaotic signals generated by this map as a function of the control parameters are also investigated. The proposed map can be used in symbolic dynamics based communication systems with advantages over current approaches based on piecewise linear maps.

**Index Terms**—Chaotic communication, chaotic maps, dynamical systems, iterative maps, Lyapunov exponent, power spectral density.

## I. INTRODUCTION

Chaotic signals are known for its irregularity, aperiodicity, decorrelation and broadband [2]. However, they can be generated by simple deterministic dynamical systems [3], which motivate their application in cryptography [4], random number generation [5], watermarking [6], communications [7] and systems modeling [8].

Chaotic signals are natural candidates for carrying information in spread-spectrum communication [2], [3]. These systems offer advantages, such as robustness to multipath propagation and low probability of interception [9]. Furthermore, chaotic signals exhibit erratic and irregular behavior providing security in the physical level.

The techniques available in the literature for the implementation of communication systems employing chaotic signals are essentially based on two methods. In the first, the information symbols are encoded into a chaotic sequence generated by a forward iteration of a chaotic map [10], [11], while the second method employs a backward iteration [12] as a way to avoid problems with error amplification and precision truncation found in the former scheme. The latter scheme is employed in a chaotic communication system [13], allowing to trade performance and security by using a piecewise linear chaotic map with a parameter that controls the length of a never visited region (known as a guard region). Other chaos-based communication systems have been proposed based on piecewise linear chaotic maps with guard region [14]–[16].

The Associate Editor coordinating the review of this manuscript and approving it for publication was Prof. Marcelo da Silva Pinho.

The authors are with the Department of Electronics and Systems, Federal University of Pernambuco, 50740-550, Recife, PE, BRAZIL, carlos.ecsouza@ufpe.br, joao.victore@ufpe.br, daniel.chaves@ufpe.br, cecilio@ufpe.br. This work received partial support from CNPq and FACEPE.

A preliminary version of this paper was presented in XXXIII Simpósio Brasileiro de Telecomunicações (SBrT15), Juiz de Fora, MG, Brazil, September 1-4, 2015 [1].

Digital Object Identifier: 10.14209/jcis.2016.9.

The guard region restricts the chaotic system dynamics due to the length of this region, which invariably induces a compromise between performance and security. This limitation is eliminated by the map proposed by the authors in [17]. This map, named the tanh map, is based on the hyperbolic tangent function and allows the creation of a guard region without chaos degradation, when quantified by the value of the Lyapunov exponent.

This work presents a new map based on the hyperbolic tangent function, named the stanh map, that generalizes the tanh map proposed in [17] with the addition of two new control parameters related to the parity and to the symmetry of the map. The stanh map has one parameter that determines the map symmetry (even or odd), one parameter that describes the location of the axis of symmetry and its shape is controlled by the parameter  $r$  that permits to change the way the system evolves. For high values of  $r$  the outputs concentrate around specific points of the attractor, whereas a seldom visited region acts as a guard region. Firstly, we study the behaviour of the Lyapunov exponent of the proposed map in terms of the control parameters. Then, we study the power spectral density of chaotic signals generated by the stanh map. Finally, we discuss a circuit implementation of the proposed map. We show that the new parameters can be used to obtain a chaotic signal with a variety of spectral characteristics, varying from low-pass to high-pass.

This paper is organized in seven sections. Section II contains a brief introduction to modulation via chaotic signals. In Section III the stanh map is introduced. The chaotic behavior of the stanh map is studied in Section IV. In Section V the spectral characteristics of the stanh map are investigated and a circuit implementation for the proposed map is discussed in Section VI. Finally, Section VII presents the conclusions.

## II. SYMBOLIC DYNAMICS MODULATION

In the beginning of the 90's the concept of chaos control [18] was introduced. In this scheme, an autonomous chaotic system dynamic is controlled through small disturbances of its orbit. The same authors proposed in [10] the application of this technique to transmit binary information, where the binary sequences are univocally mapped into orbits of the chaotic system.

Chaotic modulation techniques using symbolic dynamics were proposed in [10], [19]. The basic principle consists in creating a partitioning of the phase space and assigning a distinct symbol to every region of the partition. In this way, an information sequence is transformed into a symbol sequence

representing the visitation of the orbits in the phase space. For instance, in the case of binary sequences, the phase space is partitioned into two regions labeled with symbols 0 and 1. This partitioning is assumed throughout this work. The ideal partitioning is defined from the Poincaré sections of the map [19].

The application of chaotic maps in communication systems requires that a time series must be obtained from the iterative application of the map. Given an unidimensional map  $f(x)$ , a time series is obtained from the iteration

$$x_n = f(x_{n-1}), n = 1, 2, \dots \quad (1)$$

Given an initial condition  $x_0$ , the sequence  $\{x_i\}_{i=0}^{\infty} = \{x_0, f(x_0), f^2(x_0), \dots\}$  is called the orbit of  $x_0$  under  $f$ . Successive applications of the map are related to crossings of its orbits with an adequate Poincaré section, in a way that guarantees unique symbol sequences to the orbits. Interpreting these sequences as information symbols, they can be modulated as an orbit or as a chaotic time sequence, employing chaos control. To illustrate this method, we introduce the modified Bernoulli map [13], as shown in Fig. 1. The map  $f(x)$  is defined over a limited interval  $\mathbb{H}$  such as  $f(\mathbb{H}) = \mathbb{H}$ , so that  $\mathbb{H}$  is invariant under  $f$ . This map is piecewise-linear and induces the partitioning of  $\mathbb{H}$  into three subintervals  $I_0$ ,  $I_1$  and  $I_2$  and is defined as

$$f(x) = \begin{cases} \frac{2x+(1+p)}{1-p}, & -1 \leq x \leq -p \quad (I_0) \\ \frac{x}{p}, & -p \leq x \leq p \quad (I_1) \\ \frac{2x-(1+p)}{1-p}, & p \leq x \leq 1. \quad (I_2) \end{cases} \quad (2)$$

We define over these intervals a function  $\varphi(x)$ ,  $x \in \mathbb{H}$ , such that,  $\varphi(x) = s_0$  whenever  $x \in I_{s_0}$ ,  $0 \leq s_0 \leq 2$ . Thus,  $\varphi$  is a labeling function that identifies the subinterval where is  $x \in \mathbb{H}$ . For example, consider the point  $x$  in Fig. 1, as  $x \in I_2$  then  $\varphi(x) = 2$ .

The partitioning of  $\mathbb{H}$  can be refined with the corresponding refinement of the labelling process, such that, if  $x \in I_{s_0}$  and  $\varphi(f(x)) = s_1$ , then  $x$  is in the subinterval  $I_{s_0 s_1}$  of  $I_{s_0}$ . For example, recall that for  $x$  in Fig. 1, then  $\varphi(x) = 2$ . Applying the map on  $x$ ,  $f(x) \in I_0$ , thus  $\varphi(f(x)) = 0$  and it is possible to state that  $x$  is in the subinterval  $I_{20}$  of  $I_2$ . This induces a partition of each subinterval  $I_0$ ,  $I_1$  and  $I_2$  in three subintervals  $I_{s_0 s_1}$ ,  $0 \leq s_0, s_1 \leq 2$ . This process can be extended in the following way. If  $x \in I_{s_0 s_1 \dots s_k}$  then  $\varphi(f^i(x)) = s_i$ , for  $0 \leq s_i \leq 2$ , and  $f^0(x) = x$ , where  $0 \leq i \leq k$ . In this way, it can be shown that each point in  $\mathbb{H}$  has a unique symbolic sequence of finite length, and more, if the length of this sequence is extended to infinity, it defines a single initial condition  $x_0$  in  $\mathbb{H}$ .

The control scheme for this approach is proposed by Hayes et al. in [10]. In the iterative process, the current  $x_k$  determines the next  $M$  digits to be transmitted, for  $M$  a finite integer. From the uniqueness of the sequence of symbols  $s_k = \varphi(x_k)$ ,  $s_{k+1} = \varphi(f(x_k))$ ,  $\dots$ ,  $s_{k+M-1} = \varphi(f^{M-1}(x_k))$ , the control of the system state is a way to modulate the information symbols. For the next symbol  $s_{k+M}$  to be transmitted, the control unit calculates the necessary value of  $y$  in  $\mathbb{H}$  to generate the sequence  $s_{k+1}, \dots, s_{k+M}$ . This method is based on the

*direct forward iteration* of the expanding map given in (2) and presents two drawbacks: error amplification and precision truncation [13]. To overcome this problem the backward iteration is used, through the modified inverse Bernoulli map

$$f_s^{-1}(x) = \begin{cases} \frac{(1-p)x-(1+p)}{2}, & s = 0 \quad (I_0) \\ px, & s = 1, \quad (I_1) \\ \frac{(1-p)x+(1+p)}{2}, & s = 2, \quad (I_2) \end{cases} \quad (3)$$

which is a contraction map over  $\mathbb{H}$ . The chaotic modulation of a finite sequence of symbols  $s_n, s_{n+1} \dots s_{M-1}$  is realized by iterating (3) from a given final condition  $x_N$ . This approach is considered in diverse scenarios of chaotic communication [13]–[15]. We observe that  $f_{s_{M-1}}^{-1}(x_N) = x_{N-1} \in I_{s_{M-1}}$ , and by backward iteration the initial condition should belong to the interval  $\bigcap_{i=1}^{M-n} f_{s_{M-i}}^{-i}(\mathbb{H})$  [12]. The symbolic sequence is modulated in the chaotic signal

$$x_n = f_{s_n}^{-1}(x_{n+1}) = \dots = f_{s_n, \dots, s_{M-1}}^{-(M-n)}(x_N)$$

where  $f_{s_n, \dots, s_{M-1}}^{-(M-n)}$  is the  $(M-n)$ -th iteration of (3) given the sequence  $s_n, \dots, s_{M-1}$ . The use of a contraction map mitigates the problems of the forward iteration associated to the numerical instability and alleviates the issues of synchronization typically found in chaotic communications [11]–[13].

The procedure consists in mapping the information bit 0 to  $s = 0$  and the information bit 1 to  $s = 2$ . The inner region  $I_1$  ( $s = 1$ ) is never visited and can be interpreted as a guard region that guarantees a minimum distance between the transmitted sequences. The width of this region depends on the parameter  $p$ , making the system more robust against noise as  $p$  increases. However, the system becomes more predictable, degrading its security to cryptography. Other inconvenience of this map is the weakening of its chaotic properties by decreasing the degrees of freedom of the system from the prohibition of the occurrence of values in the region  $I_1$ .

This problem is overcome with the chaotic map based on the hyperbolic tangent function, named tanh map, introduced in [17]. This maps has a control parameter that can be conveniently tuned to maintain a region that is seldom visited (which can be interpreted as a guard region) without the need of changing the dynamics of the system by prohibiting the visitation of a region of the original map. On the other hand, the tanh map does not have spectral flexibility. This may be inadequate for applications that are frequency selective.

In the next section we define a new map, named stanh map, which is based on the tanh map with the introduction of two

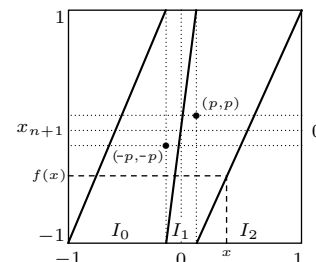


Fig. 1. The modified Bernoulli shift map.

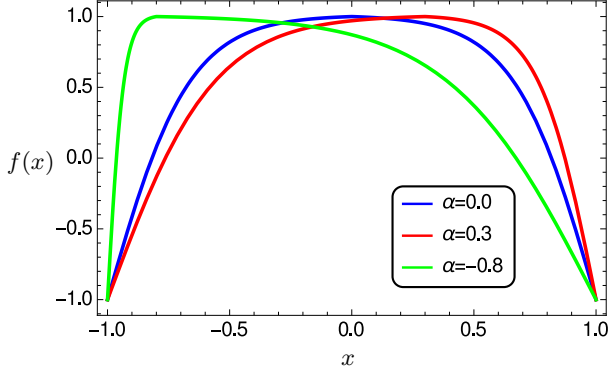


Fig. 2. The e-stanh map ( $b = 0$ ) for three values of  $\alpha$ ,  $\alpha = 0; 0.3; -0.8$ .  $r = 3$ .

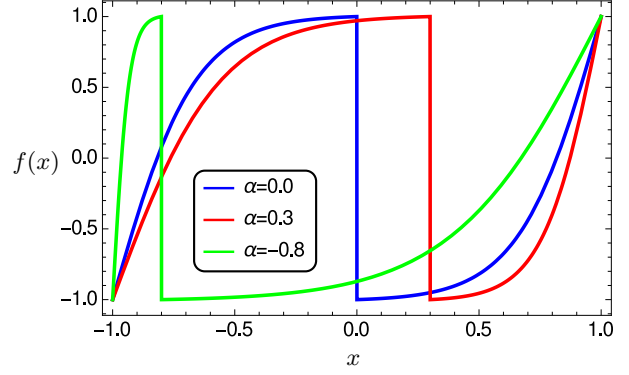


Fig. 3. The o-stanh map ( $b = 1$ ) for three values of  $\alpha$ ,  $\alpha = 0; 0.3; -0.8$ .  $r = 3$ .

new control parameters. The stanh map allows a compromise between the guard region length and frequency selectivity.

### III. THE STANH MAP

The stanh map  $f : [-1, 1] \rightarrow [-1, 1]$  is defined by

$$f(x) = \begin{cases} e \cdot \tanh\left[\frac{r}{1+\alpha} \cdot (x+1)\right] - 1, & x < \alpha \\ (-1)^b \cdot [e \cdot \tanh\left[-\frac{r}{1-\alpha} \cdot (x-1)\right] - 1] & x \geq \alpha. \end{cases} \quad (4)$$

where the scaling factor  $e$  is given by

$$e = \frac{2}{\tanh(r)}. \quad (5)$$

The control parameters are specified by the triple  $(b, r, \alpha)$ . The parameter  $b$  determines the symmetry of the stanh map and can assume the values 0 or 1. When  $b = 0$ , the stanh map has an even symmetry and is named *e-stanh*, while for  $b = 1$  the symmetry is odd and the map is named *o-stanh*. The parameter  $r$  controls the length of the guard region and assumes real values greater than zero. In this work we assume that  $r$  is defined in the interval  $(0, 10]$ . The parameter  $\alpha$  is related to the location of the axis of symmetry, which means that it shifts the central axis from  $x = 0$  to the right for positive values of  $\alpha$  and to the left for negative values of  $\alpha$ . Fig. 2 illustrates the e-stanh map for  $r = 3$  and for three values of  $\alpha$ . A similar figure for the o-stanh map is shown in Fig. 3.

When  $\alpha = 0$ , the axis of symmetry is located at  $x = 0$ , and the map is denoted by e-tanh (for  $b = 0$ ) and by o-tanh (for  $b = 1$ ). Figures 4 and 5 illustrates these two maps for three values of  $r$ . Applying the first-order Taylor series approximation  $\tanh(y) \cong y$  to (4) with  $\alpha = 0$ , the following map is derived for small values of  $r$

$$f(x) = \begin{cases} 2x + 1, & x < 0 \quad (I_0) \\ (-1)^b \cdot (-2x + 1), & x \geq 0 \quad (I_1) \end{cases} \quad (6)$$

which is the tent map for  $b = 0$  and the Bernoulli map for  $b = 1$ .

The chaotic modulation is realized through backward iteration, where the inverse of the stanh map is given by

$$f_s^{-1}(x) = \begin{cases} \frac{1+\alpha}{r} \tanh^{-1}\left(\frac{x+1}{e}\right) - 1, & s = 0 \quad (I_0) \\ -\frac{1-\alpha}{r} \tanh^{-1}\left(\frac{x+1}{be}\right) + 1, & s = 1 \quad (I_1). \end{cases} \quad (7)$$

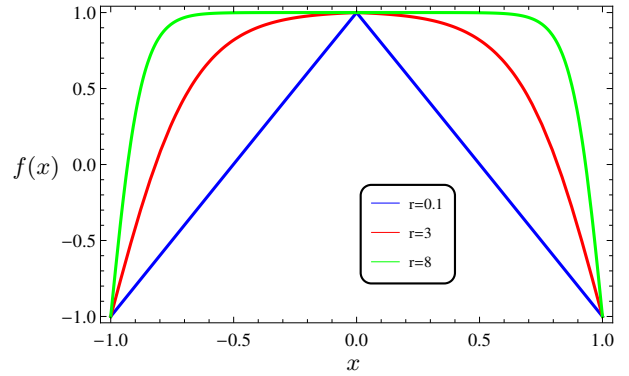


Fig. 4. The e-tanh map ( $b = 0$ ) for  $\alpha = 0$ ,  $r = 0.1; 3; 8$ .

The Lyapunov exponent of the map is analyzed in the next section.

### IV. THE CHAOTIC BEHAVIOR

The Lyapunov exponent measures the separation rate between two trajectories during the dynamic evolution of the system. Two infinitesimally close orbits tend to separate if the Lyapunov exponent is positive [2], [3]. This parameter is an indicative of presence of chaos in the system and is defined

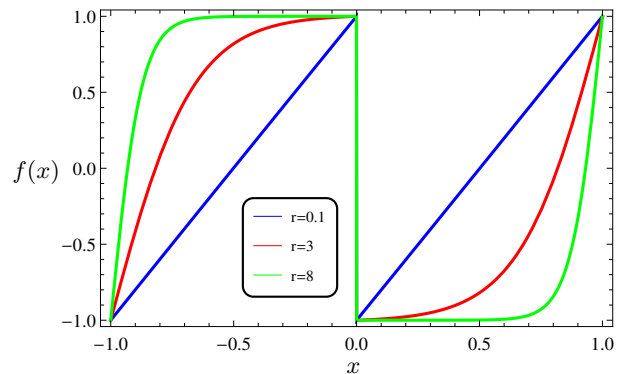
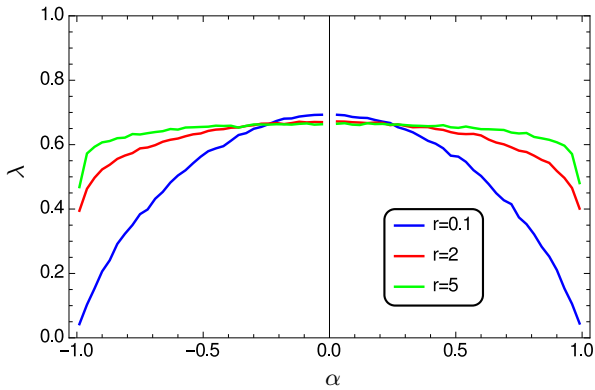
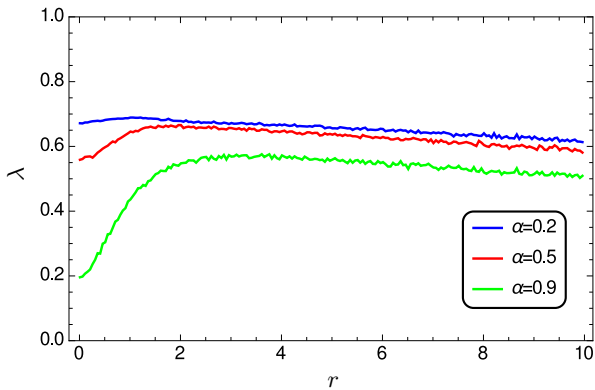


Fig. 5. The o-tanh map ( $b = 1$ ) for  $\alpha = 0$ ,  $r = 0.1; 3; 8$ .


 Fig. 6. Lyapunov exponent versus  $\alpha$  for the stanh map for  $r = 0.1; 2; 5$ .

 Fig. 7. Lyapunov exponent versus  $\alpha$  for the stanh map for  $\alpha = 0.2; 0.5; 0.9$ .

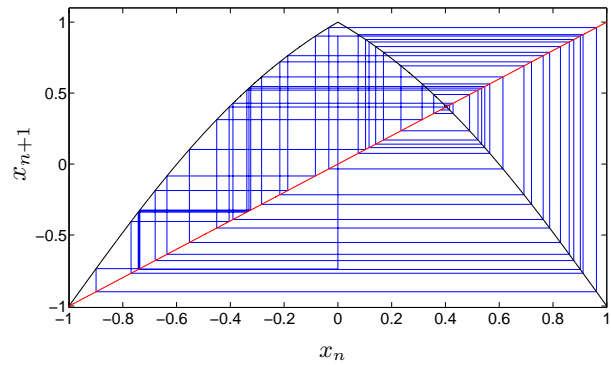
for an unidimensional discrete map as [3]

$$\lambda = \lim_{N \rightarrow \infty} \frac{1}{N} \sum_{i=0}^{N-1} \ln |f'(x_i)|. \quad (8)$$

where  $f'(x)$  is the derivative of  $f(x)$ . We show in the appendix that the Lyapunov exponent of the stanh map does not depend on  $b$ .

Figure 6 illustrates the behavior of the Lyapunov exponent versus the parameter  $\alpha$  for the stanh map for three values of the parameter  $r$ . This figure shows that the Lyapunov exponent is positive for the considered range of values of  $r$ . When  $r$  assumes values close to zero, the exponent tends to zero at the extremities of values assumed by  $\alpha$ , that is,  $|\alpha|$  close to 1. By increasing the value of  $r$ , the exponent has a more uniform variation, indicating a higher robustness of the chaos to the variation of  $\alpha$ .

Figure 7 shows how the exponent changes with  $r$  for three values of  $\alpha$ . For small values of  $r$  a higher variation of the exponent with  $\alpha$  is observed. This variations decreases as  $\alpha$  is decreased. Additionally, for sufficient high values of  $r$ , independent of  $\alpha$ , all the curves present a linear decay with a slight slope. It is observed that this property is achieved by smaller values of  $r$  as  $\alpha$  decreases. Thus, an increase in  $r$  implies that the Lyapunov exponent has less sensibility to variation of the map parameters.


 Fig. 8. Cobweb of the e-stanh map for  $r = 1$  and  $\alpha = 0$ .

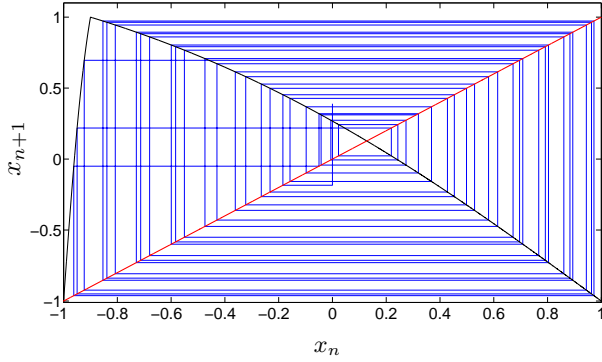
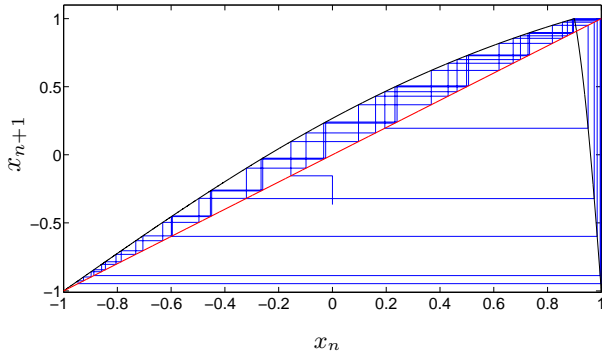
### A. Cobweb Plot

The cobweb plot is a powerful tool to qualitatively investigate the dynamics of a unidimensional map. The procedure to generate the cobweb plot is thoroughly described in [2]. Starting from  $x_0$ , we draw a vertical line connecting the point  $(x_0, 0)$  to  $(x_0, x_1)$ , then we draw a horizontal line to the diagonal point  $(x_1, x_1)$ , then go to  $(x_1, x_2)$ , the next point is  $(x_2, x_2)$ , and so on. From the cobweb plot of the e-stanh map curve in Figure 8 we can see that an input in the neighborhood of 1 ( $x_n = 1 - \delta$ ) always maps in the neighborhood of -1 ( $x_{n+1} = -1 + \delta$ ), while an input in the neighborhood of -1 maps the next point of the orbit in a negative point higher than the previous one and slowly iterate towards 1 again. As seen in Figure 9, when  $\alpha$  is negative the central area is shifted to the left increasing the derivative of the curve around -1. On the other hand, when  $\alpha$  is positive the central area is shifted to the right, as shown in Figure 10, therefore decreasing the derivative around  $x = -1$ .

We conclude from Figure 9 that a higher derivative around -1 implies that that system evolves from -1 to 1 with fewer iterations which indicates a high-frequency behavior. Furthermore, as depicted in Figure 10, we conclude that a smaller derivative around -1 implies that the system evolves slowly from -1 to 1 indicating a slow-frequency behavior. Differently from the e-stanh map, in the o-stanh map an input close to any of the extremal values maps the output to a point close to the previous input. For instance, an input close to -1 maps to an output also close to -1, thus we conclude that the transitions vary slowly. Thus, we expect a low-pass behavior and the cutoff frequency increases for an increase in  $r$ .

The cobweb plot of the o-stanh map for  $r = 5$ ,  $\alpha = 0$  is seen in Figure 11. Moreover, by changing  $\alpha$  we expect the derivative of the curve increases close to an extremity and decreases close to the other one. For instance, a negative value of  $\alpha$  increases the derivative around -1 and decreases the derivative around 1. Thus, as consequence of the odd symmetry, we expect that changes in the parameter  $\alpha$  do not significantly affect the spectral behavior of the map.

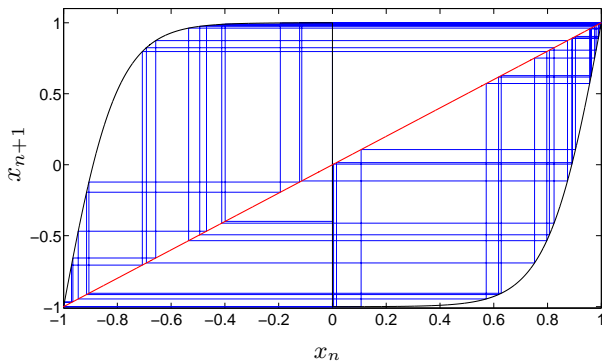
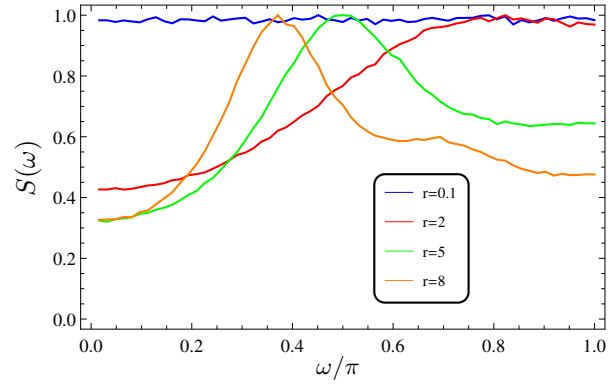
In the next section, we will evaluate the behavior of the power spectral density (PSD) of the stanh map with the variation of its parameters.


 Fig. 9. Cobweb of the e-stanh map for  $r = 1$  and  $\alpha = -0.9$ .

 Fig. 10. Cobweb of the e-stanh map for  $r = 1$  and  $\alpha = 0.9$ .

## V. SPECTRAL BEHAVIOR

The spectral characteristics of chaotic signals generated by piecewise linear maps have been investigated in [20], [21]. In this section, we investigate via computer simulations the PSD of chaotic signals produced by the stanh map.

From an initial condition  $x_0$  a finite orbit is generated  $\{x_i\}_{i=0}^{N-1}$  using (1). This orbit, which is a deterministic signal, can be considered as a sample function of a stationary stochastic process [20]. Thus,  $\{x_i\}_{i=0}^{N-1}$  is a sequence of discrete random variables indexed by  $i$  with mean  $\eta = \mathbf{E}[x_i]$  and autocorrelation function (ACF) given by  $R[m] = \mathbf{E}[x_i x_{i+m}]$ , where the expectation  $\mathbf{E}[\cdot]$  is taken over all initial conditions. For the numerical simulations of the ACF, we consider orbits


 Fig. 11. Cobweb of the o-stanh map for  $r = 5$  and  $\alpha = 0$ .

 Fig. 12. PSD of the e-tanh map ( $b = 0, \alpha = 0$ ) for  $r = 0.1; 2; 5; 8$ .  $\alpha = -0.9$ .

of length  $N = 1024$  and an ensemble of 30000 initial conditions uniformly distributed over the interval  $[-1, 1]$ .

The PSD is the discrete-time Fourier transform of the ACF

$$S(\omega) = \sum_{m=-\infty}^{\infty} R[m] e^{-j\omega m}. \quad (9)$$

If  $\eta \neq 0$ , the PSD is a sum of two parts, a periodic discrete component (spectral lines) and a continuous component (the next figures only consider this component). It is possible to obtain low-pass, high-pass and bandpass chaotic signals with the stanh map by varying the control parameters [20], [21]. We start the analysis with  $\alpha = 0$  and next we will show that a better spectrum concentration is obtained when  $\alpha$  is different from zero.

Fig. 12 shows the PSD of the ensemble generated by the e-tanh map ( $b = 0, \alpha = 0$ ) for four different values of the parameter  $r$ . The curves are normalized to a maximum value of 1. When the value of  $r$  approaches 0, the signal has a flat PSD and behaves like a white noise (this behavior is expected since the e-tanh map approximates the tent map). When  $r$  increases, the PSD varies from high-pass ( $r = 2$ ) to bandpass ( $r = 5$  and 8). On the other hand, Fig. 13 shows that the o-tanh ( $b = 1, \alpha = 0$ ) map generates low-pass signal with a bandwidth controlled by the parameter  $r$ .

Figure 14 shows the PSD of chaotic signals generated by the e-stanh map for four values of  $r$  and  $\alpha = -0.9$ . When  $r$  is small, the signal presents high-pass behavior, being more selective for smaller values of  $r$ . An increasing in  $r$  increases the passband, however the Lyapunov exponent also increases. So, high-pass signals with robust chaotic properties are generated. Finally, for values of  $r$  greater than 5 the PSD has a bandpass behavior. Figure 15 considers a positive value of  $\alpha$ , and in this case, we can see a low-pass behavior for small values of  $r$ .

To summarize, the low-pass and high-pass narrow-band behaviors of the e-stanh map are related to small values of  $r$  and positive  $\alpha$  (low-pass) or negative  $\alpha$  (high-pass). As  $r$  increases the e-stanh map assumes a bandpass behavior. Also, the higher is the value of  $r$ , the lower is the spectral dependence on the parameter  $\alpha$ .

The o-stanh map does not have the same spectral variation as the e-stanh map. Figure 16 shows that the behavior of the

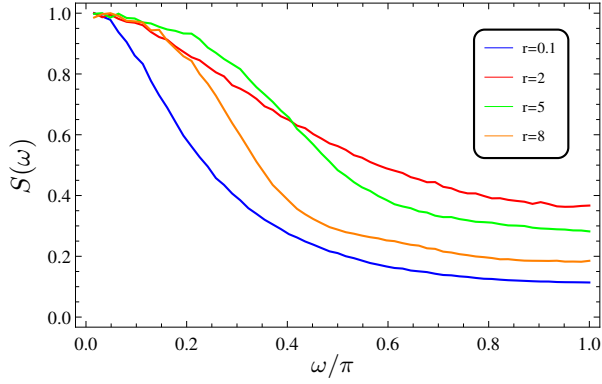


Fig. 13. PSD of the o-tanh map ( $b = 1, \alpha = 0$ ) for  $r = 0.1; 2; 5; 8$ .  $\alpha = -0.9$ .

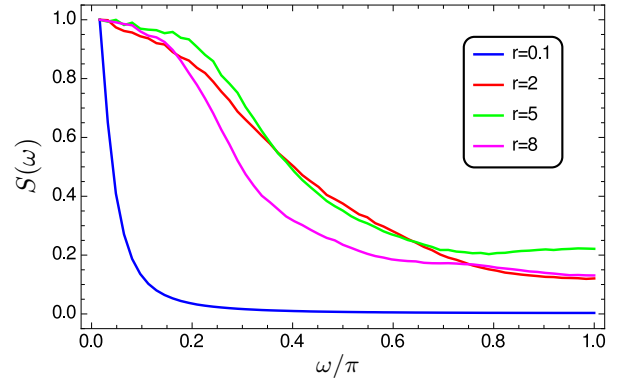


Fig. 16. PSD of the o-stanh map for  $r = 0.1; 2; 5; 8$ .  $\alpha = 0.9$ .

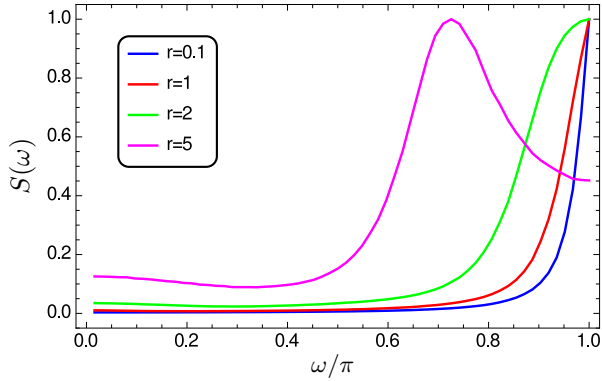


Fig. 14. PSD of the e-stanh map for  $r = 0.1; 1; 2; 5$ .  $\alpha = -0.9$ .

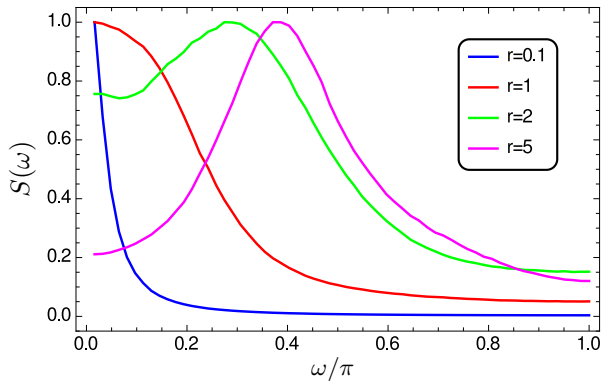


Fig. 15. PSD of the e-stanh map for  $r = 0.1; 1; 2; 5$ .  $\alpha = 0.9$ .

PSD for the o-stanh map is low-pass with higher selectivity for small values of  $r$ . It is observed (figure not shown) that this low-pass behavior is invariant to the parameter  $\alpha$ . In the next section, we present a circuit implementation of the stanh map with even symmetry ( $\alpha = 0, b = 0$ ).

## VI. CIRCUIT IMPLEMENTATION

For a circuit implementation of (4) with even symmetry (with  $\alpha = 0$  and  $b = 0$ ), we apply the following compact expression

$$f(x) = e \cdot \tanh[r \cdot (1 - |x|)] - 1. \quad (10)$$

Therefore every operation of (10) may be carried out through ordinary electronic circuits. Hereafter, the function  $f(x)$  is associated with the output current  $I_{\text{out}}$  and  $x$  with the input current  $I_{\text{in}}$  of the circuit. The collector current of a differential pair with BJT may be expressed as a hyperbolic tangent function of its differential input voltage  $v_{\text{id}}$  shown in Fig. 17. The exact expressions are well known from the theory of electronic circuit [22]

$$I_{c1} = I_{s1} \cdot \exp(v_{\text{BE1}}/V_T) \quad (11)$$

$$I_{c2} = I_{s2} \cdot \exp(v_{\text{BE2}}/V_T) \quad (12)$$

$$I_{EE} = I_{c1} + I_{c2} \quad (13)$$

where  $V_T$  is the thermal voltage,  $I_{s1}$  and  $I_{s2}$  are the reverse saturation currents of the BJT's (where  $I_{s1} = I_{s2}$ ),  $I_{EE}$  is the polarization current of the differential pair, and  $v_{\text{BE1}}$  and  $v_{\text{BE2}}$  are the base-emitter voltage of the BJT's. We express the ratio of the collector currents as

$$\frac{I_{c1}}{I_{c2}} = \exp(v_{\text{id}}/V_T) \quad (14)$$

where  $v_{\text{id}} = v_{\text{EB1}} - v_{\text{EB2}}$ . From (13) and (14) we obtain

$$I_{c2} = \frac{I_{EE}}{1 + \exp(v_{\text{id}}/V_T)}$$

that may be rewritten as

$$I_{c2} = \frac{I_{EE}}{2} \cdot \left[ 1 - \tanh\left(\frac{v_{\text{id}}}{2V_T}\right) \right]. \quad (15)$$

The output current is determined from the relation  $I_{\text{out}} + I_{c2} = I'$ , where  $I'$  is a constant that depends on the value of  $r$ . Thus, the output current is given by

$$I_{\text{out}} = \frac{I_{EE}}{2} \cdot \tanh\left(\frac{v_{\text{id}}}{2V_T}\right) - \beta \quad (16)$$

where  $\beta = I' - I_{EE}/2$ . The parameter  $\beta$  corresponds to the maximum absolute value of  $I_{\text{out}}$  that assumes values in the interval  $[-\beta, \beta]$ . Thus, the parameter  $r$  can be obtained from the relation  $I_{EE}/(2\beta) = e$ . Finally,  $v_{\text{id}}$  is a function of the input current  $I_{\text{in}}$  by the concatenation of a rectifier circuit followed by a transimpedance amplifier.

A one-dimensional discrete-time chaotic sequence can be generated from the proposed circuit by two sample-and-hold circuits, as shown in Fig. 18 for a voltage-mode configuration

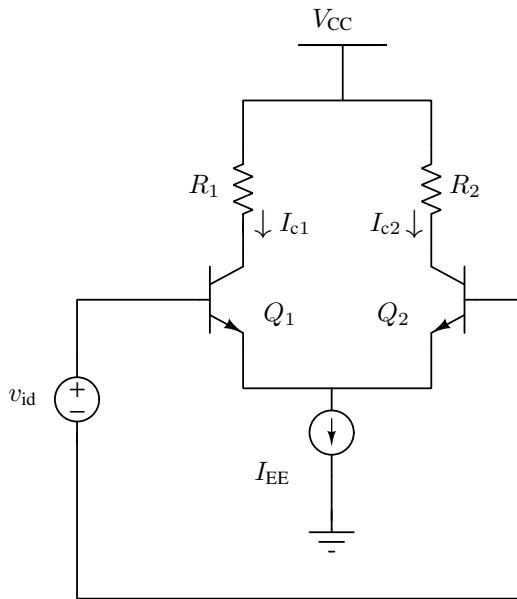


Fig. 17. Differential pair with BJT.

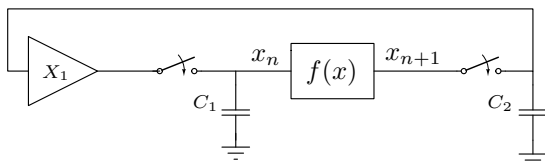


Fig. 18. Circuit diagram of the chaotic sequence generator.

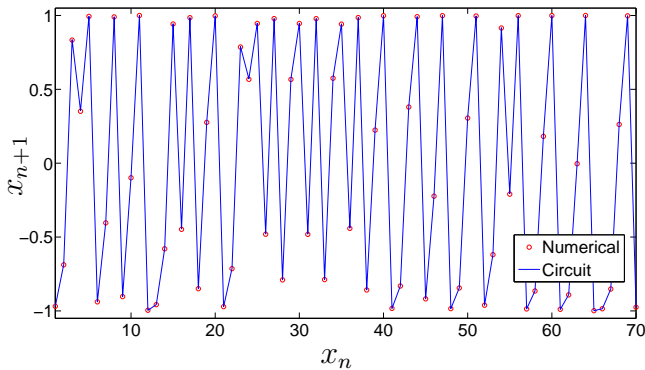


Fig. 19. Comparison between a sequence generated by a numerical simulation of the map (in red) and by the sampling of a sequence generated by the circuit simulation (in blue) for  $r = 5$ .

[23]. The block  $X_1$  in this figure corresponds to a buffer, and the block  $f(x)$  to the circuit implementation of the chaotic map.

For circuit simulation we use the NGSPICE-26. The standard model for the BJT's  $Q_1$  and  $Q_2$  of the NGSPICE-26 is used. In Fig. 19 a comparison between sequences obtained from the numerical simulation of the map and from the circuit simulations for  $r = 5$  shows that they share the same dynamical behavior.

## VII. CONCLUSIONS

From the variation of the control parameters of the stanham map it is possible to obtain chaotic signals with various spectral characteristics. The set of parameter  $(b, r, \alpha)$  can be defined to generate chaotic signals with low-pass, high-pass and bandpass spectral behavior. Beyond that, in the limit of  $r$  tending to zero, we obtain the tent map or the Bernoulli map, depending on the parity of  $f(x)$  defined by the parameter  $b$ .

The hyperbolic tangent was electronically realized through a differential pair with bipolar junction transistors [24]. By incorporating an additional circuit such as the sample-and-hold [25] and current sources, a circuit that implements the stanham map with  $\alpha = 0$  and even symmetry was simulated on SPICE, presenting a behavior in agreement with the theoretical prediction for a broad range of the parameter  $r$ . Thus, the stanham is a good candidate for applications involving information transmission and random number generation. The circuit implementation of the proposed map with odd symmetry is an interesting topic for future research.

## APPENDIX

Let  $\{x_i\}_{i=0}^{\infty}$  and  $\{y_i\}_{i=0}^{\infty}$  be two orbits generated by the e-tanh map and o-tanh map, respectively. Now, consider the supposition one that  $|x_\ell| \neq |y_\ell|$  for some  $\ell > 0$ , and the supposition two that  $x_0 = y_0$ . Observe from (4) that  $|x_{i+1}| = |y_{i+1}|$  whenever  $|x_i| = |y_i|$ , thus the supposition one is only true if  $|x_{\ell-1}| \neq |y_{\ell-1}|$ , and following a recursive reasoning we find that  $|x_0| \neq |y_0|$ , which contradicts the supposition two. It can also be shown from (4) that  $|f'(x_i)|$  (for  $b = 0$ ) is equal to  $|f'(y_i)|$  (for  $b = 1$ ) whenever  $|x_i| = |y_i|$ , and so we conclude from (8) that the Lyapunov exponent of the tanham map is invariant with the parameter  $b$ .

## REFERENCES

- [1] C. Souza, D. Chaves, and C. Pimentel, "Spectral analysis of a chaotic map based on the hyperbolic tangent function (in Portuguese)," in *XXXIII Brazilian Telecommunications Symposium*, pp. 1–5, Juiz de Fora - MG, Brazil, Sep. 2015.
- [2] S. Strogatz, *Nonlinear Dynamics and Chaos with Applications to Physics, Biology, Chemistry, and Engineering*. Studies in Nonlinearity Series, Westview Press, 2001.
- [3] K. Alligood, T. Sauer, and J. Yorke, *Chaos: An Introduction to Dynamical Systems*. Springer, NY, 1997.
- [4] L. Kocarev and S. Lian, *Chaos-based Cryptography: Theory, Algorithms and Applications*. Studies in Computational Intelligence, Springer, 2011.
- [5] T. Stojanovski and L. Kocarev, "Chaos-based random number generators-part I: analysis [cryptography]," *IEEE Trans. Circuits Syst. I Fundam. Theory Appl.*, vol. 48, pp. 281–288, Mar. 2001. doi: 10.1109/81.915385.
- [6] F. Liu and C. K. Wu, "Robust visual cryptography-based watermarking scheme for multiple cover images and multiple owners," *IET Information Security*, vol. 5, pp. 121–128, June 2011. doi: 10.1049/iet-ifs.2009.0183.
- [7] P. Stavroulakis, *Chaos Applications in Telecommunications*. Taylor & Francis, 2005.
- [8] M. Hasler, G. Mazzini, M. Ogorzalek, R. Rovatti, and G. Setti, "Scanning the special issue - special issue on applications of nonlinear dynamics to electronic and information engineering," *Proc. IEEE*, vol. 90, pp. 631–640, May 2002. doi: 10.1109/JPROC.2002.1014999.
- [9] F. Lau and C. Tse, *Chaos-Based Digital Communication Systems*. Engineering online library, Springer, 2010.
- [10] S. Hayes, C. Grebogi, and E. Ott, "Communicating with chaos," *Phys. Rev. Lett.*, vol. 70, pp. 3031–3034, May 1993. doi: 10.1103/PhysRevLett.70.3031.

- [11] C. Williams, "Robust chaotic communications exploiting waveform diversity. Part 1: Correlation detection and implicit coding," *IET Communications*, vol. 2, pp. 1213–1222, Nov. 2008. doi: 10.1049/iet-com:20070467.
- [12] J. Schweizer and T. Schimming, "Symbolic dynamics for processing chaotic signals. I. Noise reduction of chaotic sequences," *IEEE Trans. Circuits Syst. I, Fundam. Theory Appl.*, vol. 48, pp. 1269–1282, Nov. 2001. doi: 10.1109/81.964416.
- [13] D. Luengo and I. Santamaria, "Secure communications using OFDM with chaotic modulation in the subcarriers," in *IEEE Vehicular Technology Conference (VTC 2005-Spring)*, vol. 2, pp. 1022–1026, May 2005. doi: 10.1109/VETECS.2005.1543461.
- [14] G. Kaddoum, M. Vu, and F. Gagnon, "Chaotic symbolic dynamics modulation in MIMO systems," in *2012 IEEE International Symposium on Circuits and Systems (ISCAS)*, pp. 157–160, May 2012. doi: 10.1109/ISCAS.2012.6271552.
- [15] G. Kaddoum, G. Gagnon, and F. Gagnon, "Spread spectrum communication system with sequence synchronization unit using chaotic symbolic dynamics modulation," *Int. J. Bifurcat. Chaos*, vol. 23, pp. 1350019.1–1350019.14, Feb. 2013. doi: 10.1142/S0218127413500193.
- [16] G. Kaddoum, F. Gagnon, and D. Couillard, "An enhanced spectral efficiency chaos-based symbolic dynamics transceiver design," in *International Conference on Signal Processing and Communication Systems (ICSPCS)*, pp. 1–6, Dec. 2012. doi: 10.1109/ICSPCS.2012.6508021.
- [17] D. Chaves, C. Souza, and C. Pimentel, "A new map for chaotic communication," in *International Telecommunication Symposium (ITS 2014)*, pp. 1–5, Aug. 2014. doi: 10.1109/BSC.2010.5472918.
- [18] E. Ott, C. Grebogi, and J. A. Yorke, "Controlling chaos," *Phys. Rev. Lett.*, vol. 64, pp. 1196–1199, Mar 1990. doi: 10.1103/PhysRevLett.64.1196.
- [19] B. Hao and W. Zheng, *Applied Symbolic Dynamics and Chaos*. Directions in chaos, World Scientific, 1998.
- [20] M. Eisencraft, D. Kato, and L. Monteiro, "Spectral properties of chaotic signals generated by the skew tent map," *Signal Processing*, vol. 90, no. 1, pp. 385 – 390, 2010. doi: <http://dx.doi.org/10.1016/j.sigpro.2009.06.018>.
- [21] M. Eisencraft and D. M. Kato, "Spectral properties of chaotic signals with applications in communications," *Nonlinear Analysis: Theory, Methods & Applications*, vol. 71, no. 12, pp. e2592 – e2599, 2009.
- [22] P. R. Gray, P. J. Hurst, S. H. Lewis, and R. G. Meyer, *Analysis and Design of Analog Integrated Circuits, 5th Edition*. Wiley Global Education, 2009.
- [23] P. Dudek and V. Juncu, "Compact discrete-time chaos generator circuit," *Electronics Letters*, vol. 39, pp. 1431–1432, Oct. 2003. doi: 10.1049/el:20030881.
- [24] D. Pederson and K. Mayaram, *Analog Integrated Circuits for Communication: Principles, Simulation, and Design*. Kluwer Academic Publishers, 1991.
- [25] C.-C. Wang, J.-M. Huang, H.-C. Cheng, and R. Hu, "Switched-current 3-bit cmos 4.0-mhz wideband random signal generator," *Solid-State Circuits, IEEE Journal of*, vol. 40, pp. 1360–1365, June 2005. doi: 10.1109/JSSC.2005.848036.



**Carlos Souza** received the B.Sc. degree in physics from the Federal University of Pernambuco, Recife, Brazil, in 2008 and the M.Sc. degree in applied physics from the Federal Rural University of Pernambuco, Recife, Brazil, in 2013. He is currently a Ph.D. student in electrical engineering at the Federal University of Pernambuco. His current research interests include chaos communication, coding theory, information theory and random matrix theory.



**João Evangelista** received the B.Sc degree in electronics engineering from the Federal University of Pernambuco, Recife, Brazil in 2015. He is currently currently a M.Sc student at the Federal University of Pernambuco. His current research interests include chaos communications, chaotic circuits and physical layer authentication.



**Daniel Chaves** received the the B.S. degree in electronics engineering and the M.S. degree in electrical engineering from the Federal University of Pernambuco, Recife, Brazil, in 2004 and 2006, respectively, and the Ph.D. degree in electrical engineering from the State University of Campinas, So Paulo, Brazil, in 2011. In 2012, he joined the Department of Electronics and Systems, Federal University of Pernambuco, Recife, Brazil, as a Assistent Professor. His current interests include information theory, coding theory, symbolic dynamics, system modeling, chaos communication, chaotic circuits and chaos based random number generators.



**Cecilio Pimentel** was born in Recife, Brazil, in 1966. He received the B.Sc. degree from the Federal University of Pernambuco, Recife, Brazil, in 1987; the M.Sc. degree from the Catholics University of Rio de Janeiro, Rio de Janeiro, Brazil, in 1990; and the Ph.D. degree from the University of Waterloo, Ontario, Canada, in 1996, all in electrical engineering. Since October 1996, he has been with the Department of Electronics and Systems at the Federal University of Pernambuco, where he is currently an Associate Professor. From 2007 to 2008, he was a Visiting Research Scholar at the Department of Mathematics and Statistics, Queen's University, Kingston, Canada. His research interests include digital communications, information theory, and error correcting coding.